Gold Nanostructures

DOI: 10.1002/anie.200703259

# Chemical Sharpening of Gold Nanorods: The Rod-to-Octahedron Transition**

*Enrique Carbó-Argibay, Benito Rodríguez-González, Jessica Pacifico, Isabel Pastoriza-Santos,* Jorge Pérez-Juste, and Luis M. Liz-Marzán**

Morphology control at the nanoscale is a hot topic because of the spectacular effects that small changes in the shape of nanoparticles can have on a variety of physical properties of the material.[1] In particular, metal nanoparticles have been shown to display interesting optical properties related with the oscillation of conduction electrons, in resonance with incoming light, the so-called surface plasmon resonances.[2] The specific resonance frequencies of plasmon modes in metal nanoparticles are strongly dependent on their morphology,[3] which has driven intensive research towards their size and shape control.[4] A large number of synthetic methods based on colloid chemistry have been developed for the production of particles with different shapes, and there is a strong debate regarding the specific mechanisms involved in anisotropic growth.[5] In general, metals (most of them with a cubic structure) tend to nucleate and grow into thermodynamically stable nanoparticles with their surfaces bound by the low-energy facets so as to minimize the total surface energy.[6] Nevertheless, highly anisotropic shapes, not favorable from the perspective of thermodynamics, have been obtained by the introduction of capping agents which can alter the surface energies for the different crystallographic planes.[7] Herein, we present evidence of tip sharpening and reshaping during the growth of gold nanorods, with a complete conversion from spherically capped cylinders into single-crystal octahedrons. A detailed study of the growth process reveals a gradual change in the morphology of the particles directly related with the faster growth of certain crystallographic facets. Fine-tuning of the reaction conditions allows the isolation of nanoparticle colloids with a variety of intermediate shapes, in turn leading to a variation of the relative intensities and positions of longitudinal and transverse surface plasmon modes.

[*] E. Carbó-Argibay, Dr. B. Rodríguez-González, Dr. J. Pacifico, Dr. I. Pastoriza-Santos, Dr. J. Pérez-Juste, Prof. L. M. Liz-Marzán
Departamento de Química Física and Unidad Asociada CSIC
Universidade de Vigo
36310, Vigo (Spain)
Fax: (+34) 986-812-556
E-mail: pastoriza@uvigo.es
lmarzan@uvigo.es

[**] I.P.-S. acknowledges the Isidro Parga Pondal Program (Xunta de Galicia, Spain). J.P.-J. acknowledges the Santiago Ramón y Cajal Program (MEC, Spain). This work was supported by the Spanish Ministerio de Educación y Ciencia (grant MAT2003-02991), Xunta de Galicia, and COST Action D43.

Supporting information for this article is available on the WWW under http://www.angewandte.org or from the author.

The chemical process involved in the reshaping process starts from single-crystal gold nanorods synthesized by seed-mediated growth in aqueous solution. These rods are in turn used as seeds for further growth in the ultrasound-induced reduction of $HAuCl_4$ by *N*,*N*-dimethylformamide (DMF), in the presence of poly(vinylpyrrolidone) (PVP), as previously described for the growth of regular gold nanodecahedra on premade, small seeds.[8] Although PVP has been often claimed to be a shape-directing agent,[9] a variety of morphologies have been obtained with this polymer. However, we have demonstrated in our previous work that the seed not only serves as a catalyst for gold reduction but also determines the crystallographic structure and geometry of the final particles, so that pentagonal bipyramids (decahedrons) were obtained from penta-twinned Au seeds, whereas the growth of single-crystal Pt seeds yielded perfect octahedrons. This observation was in agreement with previous reports from a number of groups[5b,10] using a variety of preparation protocols. The use of nanorods as seeds arises as a possibility to manipulate their dimensions in a controlled manner, with the aim of fine-tuning their optical response. The single-crystal nanorods used here were synthesized by seeded growth in aqueous cetyltrimethylammonium bromide (CTAB) solution[5b,11] (see Experimental Section for details) and had an average aspect ratio of 4.2 [$(60.8 \pm 8.7)$ nm × $(15.1 \pm 3.6)$ nm]. Prior to the growth experiment, CTAB was exchanged with poly(vinylpirrolidone) (PVP) as previously reported[12] to allow transfer into DMF with no aggregation. As the Au nanorods are known to reshape at moderate temperatures,[13] control heating experiments were carried out to avoid significant thermal reshaping during growth for which the reaction temperature was set around 75 °C (see Supporting Information for further details on thermal reshaping).

Figure 1 shows the time evolution of the UV/Vis spectra during the growth of Au nanorods (2.92 μmol Au atoms) in 15 mL of a DMF solution containing $HAuCl_4$ (2.5 mM) and PVP (2.5 mM) previously sonicated for 1 h to reduce $Au^{III}$ into $Au^{I}$ (see Experimental Section). The extinction spectrum of the initial nanorod dispersion displays a longitudinal surface plasmon resonance (SPR) band centered at 861 nm and a weak transverse SPR band at 513 nm. During the process, the longitudinal SPR band gradually undergoes a blue shift, while the transverse SPR undergoes a red shift and is significantly enhanced. Gradually, both bands merge into a single band centered at 570 nm that subsequently undergoes a red shift and gain in intensity. Transmission electron microscopy (TEM) analysis of aliquots withdrawn at different reaction times reveals that the observed spectral evolution arises from

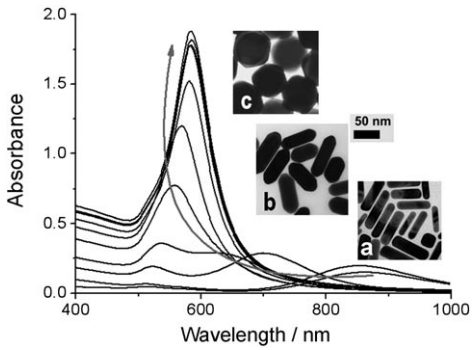


***Figure 1.*** Time evolution of UV/Vis spectra during the growth of Au nanorods in DMF (2.5 mM $HAuCl_4$ and 2.5 mM PVP) at 75 °C under sonication. The total reaction time was 3 h. The arrow shows the progress of the reaction. Insets: TEM images showing the morphology of the Au nanoparticles in samples withdrawn at different reaction times: a) 0; b) 100, and c) 180 min. Scale bar: 50 nm for all images.

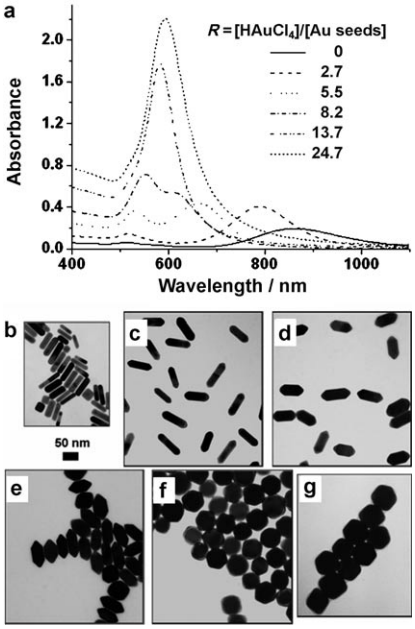


***Figure 2.*** a) UV/Vis spectra of Au nanorods used as seeds (solid line) and after their growth with different amounts of $HAuCl_4$ ($R$) as indicated. b–g) TEM images of Au nanorods used as seeds (b) and the final products obtained at different $R$ values: c) 2.7, d) 5.5, e) 8.2, f) 13.7, and g) 24.7. Scale bar: 50 nm for all images.

morphological changes of the particles that result in a steady decrease of the aspect ratio but also in sharpening and formation of acute apexes, which eventually results in a complete conversion of the rods into octahedrons (see insets in Figure 1). These observations are in good agreement with the optical measurements, with the initial blue shift of the longitudinal SPR attributed to the decreasing aspect ratio owing to the formation of thicker rods[4a] and the final red shift of the single band attributed to the growth of the resultant octahedral nanoparticles.[14]

The same procedure can be conveniently modified to fabricate nanoparticles with a range of intermediate morphologies (between rod and octahedron) and optical properties by simply varying the $HAuCl_4$/Au seed concentration ratio ($R$). Representative UV/Vis spectra (Figure 2a) and corresponding TEM images (Figure 2b–g) are given in Figure 2 for the final products obtained by reacting a constant amount of Au seed (2.92 μmol Au) with different amounts of $HAuCl_4$, thus changing $R$. (Details concerning the dimensions of the nanoparticles obtained in this particular series can be found in Table 1 in the Supporting Information.) It can be observed that at low $R$ values ($R = 2.7$) the obtained particles maintain a rodlike morphology but with larger dimensions, a slightly lower aspect ratio (3.8 vs 4.2 for the starting rods), and notably sharper tips (Figure 2c). The reduction in aspect ratio is reflected in a small blue shift of the longitudinal SPR (LSPR). When higher $HAuCl_4$ concentrations are used ($R = 5.5$ and $R = 8.2$), the resulting particles are clearly thicker (see Table 1 in the Supporting Information, and Figure 2d,e). Accordingly, the blue shift of the LSPR is now much larger so that the LSPR starts to merge with the transverse SPR (see Figure 2a). Finally, at $R > 13.7$, the particles become perfect octahedrons (Figure 2f,g) with an aspect ratio of 1, in agreement with the observed spectra, which undergo a red shift as the particle size is increased.[14]

To understand the mechanisms involved in this reshaping process, the specific morphology and crystalline structure of the particles formed using various $R$ values (0, 2.7, 8.2, 13.7) were analyzed by TEM and atomic force microscopy (AFM). Figure 3 shows that in all cases, regardless of the $R$ value, the

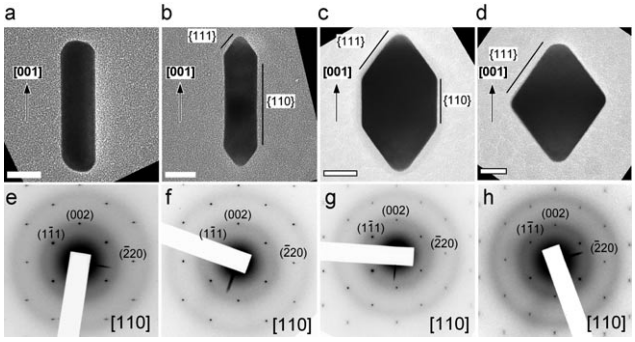


***Figure 3.*** a–d) Representative TEM images of the original nanorods (a) and particles obtained with $R = 2.7$ (b), $R = 8.2$ (c), and $R = 13.7$ (d). All particles are oriented along the [001] direction, as indicated by arrows. e–h) Corresponding electron diffraction patterns of the displayed particles demonstrating their single-crystallinity; electron diffraction rotations are compensated. Scale bars: 20 nm.

single-crystalline fcc structure of the original nanorods is maintained, as demonstrated by the corresponding selected area electron diffraction (SAED) patterns. It has been reported that for similar single-crystal Au nanorods synthesized by the electrochemical method, the lateral facets are dominated by the {110} planes of the fcc lattice linked to each other by smaller {100} facets (eight in total), whereas the rod tips are terminated by {100}, {110}, and {111} facets.[15] For comparison, we carried out tilting experiments within the TEM on the initial nanorods and the different final particles (Figure 4). The cross-section of the initial nanorods was found to be nearly rounded, resembling the octagonal section predicted in reference [15]. This is confirmed by the rounded

  

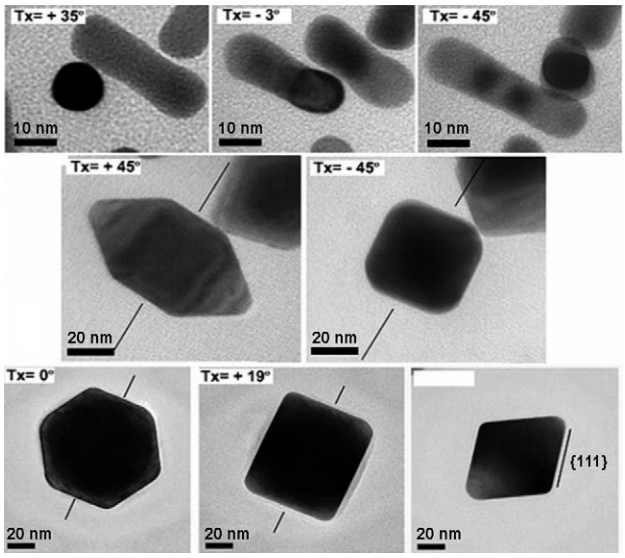


***Figure 4.*** TEM images from an original rod (top), a sharpened rod (middle), and an octahedron (bottom) tilted on the TEM grid at different angles (Tx).

shape of the particles determined from the AFM topographic profiles shown in Figure 5. However, for the intermediate rods with sharp apexes, TEM tilting experiments (Figure 4) and acoustic intermittent (AC) mode AFM imaging (Figure 5) both nicely show that the particles have a nearly

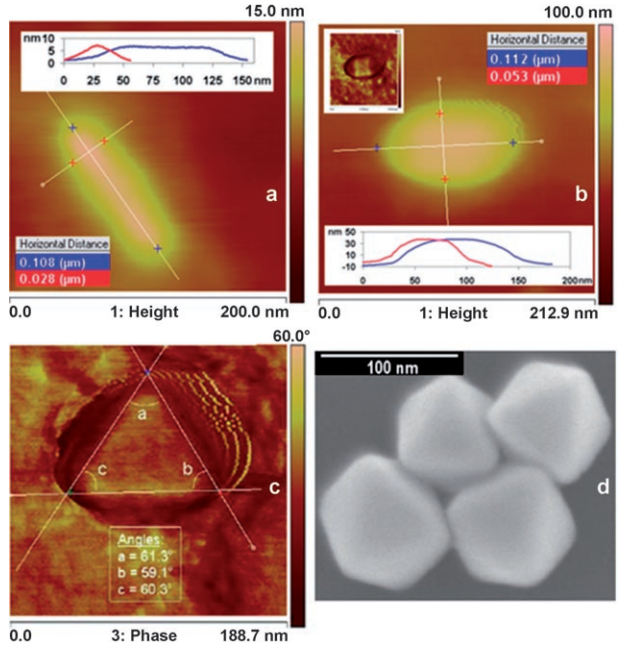


***Figure 5.*** (a–c) AFM images of a starting nanorod (a), a sharpened rod (b), and an octahedron (c). The dimensions of the particles (a,b, insets) were calculated from the AC mode AFM topographic images, using the exact section of their profile. Horizontal distances are indicated in the tables (a,b). The phase imaging scan contributed to the calculations in the case of the sharpened rod (b) and allowed the angle calculations for the octahedron (c) by providing a better defined image. The octahedral shape was confirmed by SEM (d).

square cross-section, with flat, rectangular lateral faces terminated in four well-defined, tilted faces at each tip. Further SAED analysis (Figure 3) reveals that the tips are composed of {111} facets and indicates that the lateral facets are {110} (see Supporting Information for details). The octahedral morphology of the particles obtained with high $R$ values was also confirmed by tilting TEM (Figure 4; see Supporting Information also) and SAED for the different particle orientations,[8] and by AFM and SEM (Figure 5).

The morphological characterization described above indicates that when a sufficient amount of Au is reduced on the starting nanorods, they initially reshape through sharpening of the tips and faceting of the cross-section from (rounded) octagonal into tetragonal (with slightly rounded edges), eventually leading to formation of perfect octahedrons, while maintaining a single-crystalline structure during the whole growth process. On the basis of these morphological changes, we propose a growth mechanism as sketched in Figure 6. The initial rods are enclosed within eight {110} and

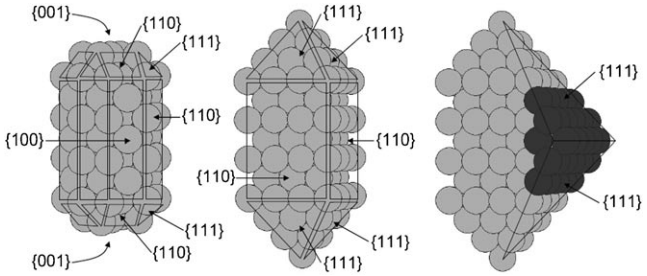


***Figure 6.*** Structural model of Au nanorod growth. Left: Original nanorod with octagonal cross-section and {100}, {110}, {111} facets. Center: Rod with sharp tips, square cross-section, {110} and {111} facets. Right: Growth of a sharpened rod into an octahedral particle by deposition of Au atoms (dark spheres) along the {110} facets.

{100} alternating lateral facets, their tips being terminated by {100}, {110}, and {111} facets (Figure 6a). Transformation into particles with four {110} lateral facets and sharp tips enclosed by four {111} facets (Figure 6b) should involve disappearance of the {100} side facets through preferential addition of Au atoms on them, so that the edges approach each other, with the {110} facets growing at their expense. The morphological transition produced by further growth of the sharp nanorods will accordingly be determined by the ratio between the growth rates along the [110] and the [111] directions, as these rods only have {110} (at the sides) and {111} (at the tips) faces. This is schematically shown in Figure 6c by the dark spheres closing the {110} facet and forcing the {111} facets to join with each other in the final octahedral structure.

The described mechanism, based on preferential growth of certain crystalline facets should correlate with a sequence of surface energies in the order $\{100\} > \{110\} > \{111\}$, which is not in full agreement with the general sequence of surface energies for the different crystallographic Au fcc planes $\gamma(111) < \gamma(100) < \gamma(110)$.[6,16] However, the precise values of the respective surface energies can be significantly affected by the adsorption of chemical species such as ions or capping molecules, and thus, for example, PVP adsorption may be

  

responsible for such changes and would explain the frequent claim that PVP plays a key role on shape control during nanoparticle growth.[4c,17]

An additional factor that may affect the growth mode of the rods is the balance of charges on each nanocrystal which should lead to symmetrical attachment of atoms to maintain the particle surface charge. This is in agreement with the previously claimed influence of the electric field distribution around the particle, as discussed in reference [5d].

In summary, the shape of (single-crystal) gold nanorods can be finely tuned by controlled growth under sonication in DMF in the presence of PVP. Reshaping involves the formation of rods with sharp tips and strongly faceted lateral faces and ultimately leads to perfect single-crystal octahedrons. Careful analysis of the morphological and crystallographic structure of the different particles indicates that the growth rate on different facets follows the order $\{111\} < \{110\} < \{100\}$, which requires PVP adsorption to alter the surface energies of bare fcc faces. This result is thus in favor of a shape-inducing effect of the polymer through different binding interactions for the different faces, as has been previously indicated by several researchers. The results are also in complete agreement with previous results by us[8] and others,[5b] indicating that the crystallographic structure of the seeds plays a key role in determining the final structure and shape of the nanoparticles grown on them.

Apart from the mechanistic value of the results reported here, the formation of sharp tips and edges in the obtained nanoparticles suggests that near-field enhancement at such spots can be very high, as compared to nanorods with rounded edges, and they can thus find applications in fields such as biosensing[18] and surface-enhanced Raman spectroscopy (SERS).[19] Detailed optical characterization and modeling is underway and will be reported elsewhere. Additionally, sharpening of Au tips can also become a critical part of self-organization processes at the nanoscale because of the variation in the electric field distribution,[5d] in a similar fashion to the anisotropic assembly of CdTe nanoparticles.[20]

## Experimental Section

Materials: Tetrachloroauric acid ($HAuCl_4 \times 3H_2O$), silver nitrate ($AgNO_3$), sodium borohydride ($NaBH_4$), ascorbic acid, concentrated HCl, and cetyltrimethyl ammonium bromide (CTAB) were purchased from Aldrich. Poly(vinylpyrrolidone) (PVP, $M_r = 40000$) was supplied by Fluka. All chemicals were used as received. Milli-Q deionized water (resistivity $> 18\ M\Omega\,cm^{-1}$) and ethanol were used for all preparations.

Nanorod synthesis: A solution of gold seed was prepared by borohydride reduction of $HAuCl_4$ (0.25 mM, 5 mL) in aqueous CTAB solution (0.1M). The average particle size measured from TEM was $(2.8 \pm 0.7)$ nm. An aliquot of seed solution (24 μL) was added to a growth solution (10 mL) containing CTAB (0.1M), $HAuCl_4$ (0.5 mM), ascorbic acid (0.8 mM), silver nitrate (0.12 mM), and HCl (18.6 mM). The dimensions of the gold nanorods measured from TEM were $(60.8 \pm 8.7)\ nm \times (15.1 \pm 3.6)$ nm, with an aspect ratio of $4.2 \pm 0.6$.

PVP coating: Typically, a suspension of as-prepared gold nanorods (10 mL) was centrifuged at 8000 rpm for 20 min, the supernatant was discarded, and the precipitate was redispersed in Milli-Q water (5 mL). Subsequently, an aliquot of CTAB-coated gold nanorods (5 mL) was mixed with an aqueous solution of PVP (1.2 mM, 5 mL) and stirred overnight. The mixture was centrifuged at 4500 rpm for 80 min, the clear supernatant was discarded, and the precipitate was redispersed in water (0.2 mL). Ethanol (1 mL) was added to the aqueous dispersion of PVP-coated gold nanorods under vigorous stirring. The concentration in terms of gold at this stage was approximately 2.92 mM.

Growth of the gold nanorods: Before adding the premade seed solution, an aqueous $HAuCl_4$ solution (0.1136M) was added to a solution of PVP in DMF (2.5 mM, 15 mL) in a 50-mL vessel. The concentration of $Au^{3+}$ ranged between 0.5 and 4.5 mM. The mixture was sonicated until reduction of $Au^{3+}$ into $Au^{+}$ was complete (disappearance of the $Au^{3+}$ UV/Vis absorption band at 325 nm). Once all the $Au^{3+}$ had been reduced, an aliquot of the rod solution (1 mL) was added and further ultrasonic irradiation was allowed until the process was finished. Ultrasonic irradiation was performed with a Bandelin Sonopuls HD2200 ultrasonic homogenizer operating at the frequency of 20 kHz and at 15% of the maximum power (200 W) to maintain the solution temperature at 75°C during the process.

Characterization: UV/Vis spectra were recorded using a Cary 5000 UV-Vis-NIR spectrophotometer. Measurements were made every 10 min after the reaction was initiated, by stopping the process and withdrawing aliquots and diluting whenever required.

A JEOL JEM 1010 transmission electron microscope operating at an acceleration voltage of 100 kV was used for low-magnification imaging. SAED images were obtained with a JEOL JEM 2010 FEG-TEM operating at an acceleration voltage of 200 kV. A Philips CM20 microscope operating at 200 kV was used for the tilting experiments. The samples for TEM were centrifuged at 3500 rpm three times and redispersed in ethanol to avoid the dissolution of the polymer layer on the TEM grid by DMF and to decrease the PVP concentration. AC AFM images were collected with a Digital Instruments Multimode V, using a Veeco RTESP tip with a resonance frequency of 295 kHz and a spring constant of $k = 50\ N\,m^{-1}$.

Received: July 20, 2007
Revised: August 14, 2007
Published online: October 25, 2007

**Keywords:** crystal growth · gold · nanostructures · shape control

[1] a) M.-C. Daniel, D. Astruc, *Chem. Rev.* **2004**, *104*, 293–346; b) C. Burda, X. Chen, R. Narayanan, M. A. El-Sayed, *Chem. Rev.* **2005**, *105*, 1025–1102; c) J. A. Dahl, B. L. S. Maddux, J. E. Hutchison, *Chem. Rev.* **2007**, *107*, 2228–2269; d) A.-H. Lu, E. L. Salabas, F. Schüth, *Angew. Chem.* **2007**, *119*, 1242–1266; *Angew. Chem. Int. Ed.* **2007**, *46*, 1222–1244.

[2] U. Kreibig, M. Vollmer, *Optical Properties of Metal Clusters*, Springer, Berlin, **1996**.

[3] a) P. Mulvaney, *Langmuir* **1996**, *12*, 788–800; b) K. L. Kelly, E. Coronado, L. L. Zhao, G. C. Schatz, *J. Phys. Chem. B* **2003**, *107*, 668–677; c) C. Nóguez, *J. Phys. Chem. C* **2007**, *111*, 3806–3819.

[4] a) J. Pérez-Juste, I. Pastoriza-Santos, L. M. Liz-Marzán, P. Mulvaney, *Coord. Chem. Rev.* **2005**, *249*, 1870–1901; b) M. P. Pileni, *J. Phys. Chem. C* **2007**, *111*, 9019–9038; c) B. Wiley, Y. Sun, B. Mayers, Y. Xia, *Chem. Eur. J.* **2005**, *11*, 454–463; d) L. M. Liz-Marzán, *Langmuir* **2006**, *22*, 32–41.

[5] a) V. Bastys, I. Pastoriza-Santos, B. Rodríguez-González, R. Vaisnoras, L. M. Liz-Marzán, *Adv. Funct. Mater.* **2006**, *16*, 766–773; b) M. Liu, P. Guyot-Sionnest, *J. Phys. Chem. B* **2005**, *109*, 22192–22200; c) Y. Sun, B. Mayers, T. Herricks, Y. Xia, *Nano Lett.* **2003**, *3*, 955–960; d) J. Pérez-Juste, L. M. Liz-Marzán, S. Carnie, D. Y. C. Carnie, P. Mulvaney, *Adv. Funct. Mater.* **2004**, *14*, 571–579; e) M. P. Pileni, *J. Exp. Nanosci.* **2006**, *1*, 13–27.

[6] L. D. Marks, *Rep. Prog. Phys.* **1994**, *57*, 603–649.

[7] a) M. P. Pileni, *Nat. Mater.* **2003**, *2*, 145–150; b) Y. Xiong, H. Cai, B. J. Wiley, J. Wang, M. J. Kim, Y. Xia, *J. Am. Chem. Soc.* **2007**,

  

*129*, 3665 – 3675; c) Y. Xiang, X. Wu, D. Liu, X. Jiang, W. Chu, Z. Li, Y. Ma, W. Zhou, S. Xie, *Nano Lett.* **2006**, *6*, 2290 – 2294.
[8] A. Sánchez-Iglesias, I. Pastoriza-Santos, J. Pérez-Juste, F. J. García de Abajo, L. M. Liz-Marzán, *Adv. Mater.* **2006**, *18*, 2529 – 2534.
[9] a) I. Pastoriza-Santos, L. M. Liz-Marzán, *Langmuir* **2002**, *18*, 2888 – 2894; b) C. E. Hoppe, M. Lazzari, I. Pardiñas-Blanco, M. A. López-Quintela, *Langmuir* **2006**, *22*, 7027 – 7034; c) I. Washio, Y. J. Xiong, Y. D. Yin, Y. N. Xia, *Adv. Mater.* **2006**, *18*, 1745 – 1749.
[10] a) J. L. Elechiguerra, J. Reyes-Gasga, M. J. Yacaman, *J. Mater. Chem.* **2006**, *16*, 3906 – 3919; b) P. L. Gai, M. A. Hammer, *Nano Lett.* **2002**, *2*, 771 – 774; c) C. J. Johnson, E. Dujardin, S. A. Davis, C. J. Murphy, S. Mann, *J. Mater. Chem.* **2002**, *12*, 1765 – 1770; d) B. Wiley, T. Herricks, Y. Sun, Y. Xia, *Nano Lett.* **2004**, *4*, 1733 – 1739; e) V. Germain, J. Li, D. Ingert, Z. L. Wang, M. P. Pileni, *J. Phys. Chem. B* **2003**, *107*, 8717 – 8720; f) C. Lofton, W. Sigmund, *Adv. Funct. Mater.* **2005**, *15*, 1197 – 1208.
[11] B. Nikoobakht, M. A. El-Sayed, *Chem. Mater.* **2003**, *15*, 1957 – 1962.
[12] I. Pastoriza-Santos, D. Gomez, J. Pérez-Juste, L. M. Liz-Marzán, P. Mulvaney, *Phys. Chem. Chem. Phys.* **2004**, *6*, 5056 – 5060.
[13] H. Petrova, J. Pérez-Juste, I. Pastoriza-Santos, G. V. Hartland, L. M. Liz-Marzán, P. Mulvaney, *Phys. Chem. Chem. Phys.* **2006**, *8*, 814 – 821.
[14] C. Li, K. L. Shuford, Q.-H. Park, W. Cai, Y. Li, E. J. Lee, S. O. Cho, *Angew. Chem.* **2007**, *119*, 3328 – 3332; *Angew. Chem. Int. Ed.* **2007**, *46*, 3264 – 3268.
[15] Z. L. Wang, M. B. Mohamed, S. Link, M. A. El-Sayed, *Surf. Sci.* **1999**, *440*, 809 – 814.
[16] Z. L. Wang, *J. Phys. Chem. B* **2000**, *104*, 1153 – 1175.
[17] F. Kim, S. Connor, H. Song, T. Kuykendall, P. Yang, *Angew. Chem.* **2004**, *116*, 3759; *Angew. Chem. Int. Ed.* **2004**, *43*, 3673 – 3677.
[18] A. J. Haes, R. P. Van Duyne, *Anal. Bioanal. Chem.* **2004**, *379*, 920 – 930.
[19] W. E. Doering, S. Nie, *J. Phys. Chem. B* **2002**, *106*, 311 – 317.
[20] Z. Y. Tang, M. Giersig, N. A. Kotov, *Science* **2002**, *297*, 237 – 240.

  